

**$\gamma$  spectroscopy of  $^{25,27}\text{Ne}$  and  $^{26,27}\text{Na}$** 

A. Obertelli, A. Gillibert, N. Alamanos, M. A. G. Alvarez,\* F. Auger, R. Dayras, A. Drouart, N. Keeley, V. Lapoux, X. Mougeot, L. Nalpas, E. Pollacco, F. Skaza, and Ch. Theisen  
CEA-SACLAY DSM/DAPNIA/SPhN F-91191 Gif-sur-Yvette, France

G. de France, B. Jurado,† W. Mittig, F. Rejmund, M. Rejmund, P. Roussel-Chomaz, and H. Savajols  
GANIL BP 5027, F-14076 Caen cedex 5, France

A. Pakou and N. Patronis

Department of Physics, The University of Ioannina, 45110 Ioannina, Greece

(Received 24 March 2006; revised manuscript received 19 October 2006; published 7 December 2006)

The  $\gamma$  spectroscopy of  $^{25,27}\text{Ne}$  and  $^{26,27}\text{Na}$  was studied from the reaction of  $^{26}\text{Ne}$  with a deuterium target in inverse kinematics at 9.7 MeV/nucleon. The selectivity of the  $(d, p)$ ,  $(d, t)$ , and  $(d, n)$  transfer reactions provides new spectroscopic information on low-lying states. The validity of the  $sd$  shell-model space for these nuclei is discussed.

DOI: [10.1103/PhysRevC.74.064305](https://doi.org/10.1103/PhysRevC.74.064305)

PACS number(s): 25.60.-t, 21.10.Pc, 23.20.Lv, 27.30.+t

## I. INTRODUCTION

Two strong isospin-dependent phenomena involving the orbitals from the  $sd$  and  $fp$  shells have been experimentally suggested in the neutron-rich region for masses  $20 \leq A \leq 40$ : the disappearance of the  $N = 20$  magic number and the appearance of  $N = 16$  as a new magic number. The first indication of the weakening of the  $N = 20$  shell closure has been given through mass measurements of sodium and magnesium isotopes [1,2]. The low excitation energy of the first  $2^+$  state [3] and the high reduced transition probability  $B(E2)$  [4] of  $^{32}\text{Mg}$  can only be reproduced assuming an intruder configuration ( $2\hbar\omega$ ) with two neutrons in the  $fp$  shell for the ground state [5], showing that  $^{32}\text{Mg}$  is deformed. The same feature is suggested for  $^{30}\text{Ne}$  from a  $(p, p')$  measurement in inverse kinematics [6].  $N = 16$  has been experimentally [7,8] suggested to be a possible magic number in the vicinity of  $^{24}\text{O}$ , as already predicted by several models [9–11]. This is interpreted as an enhancement of the spherical gap between the  $s_{1/2}$  and the  $d_{3/2}$  subshells of the neutron  $sd$  shell compared to its value for stable nuclei or as proton-neutron correlation effects [10]. In the latter description, the  $sd$ - $fp$  shell gap is predicted to be considerably reduced compared to stability. Data are needed to clearly determine the shell structure of neutron-rich nuclei in the  $N = 16$  to  $N = 20$  region where both deformation and spherical shell gap evolution are expected to coexist. In this article, we report on the  $\gamma$  spectroscopy of  $^{25,27}\text{Ne}$  and  $^{26,27}\text{Na}$  from the reaction of  $^{26}\text{Ne}$  with a deuterium target at 9.7 MeV/nucleon. New spectroscopic information about  $^{25}\text{Ne}$ , together with previous results for  $^{27}\text{Ne}$  [12], allow studying the intrusion of  $fp$  orbitals along the neon isotopic chain. The results obtained for  $^{26,27}\text{Na}$

confirm the validity of the  $sd$  shell-model space for these neutron-rich sodium isotopes.

## II. EXPERIMENTAL SETUP

The experiment was performed using the SPIRAL facility [13] of GANIL (Grand Accélérateur National d'Ions Lourds). A  $^{26}\text{Ne}$  beam was produced via an ISOL method: a  $^{36}\text{S}$  primary beam of 1 kW at 77.5 A MeV was fragmented and stopped in the thick carbon SPIRAL target. After the selection and acceleration by the CIME cyclotron, a pure  $^{26}\text{Ne}$  secondary beam was delivered at 9.7 MeV/nucleon with an intensity of  $\sim 3000$  pps. The charge state  $^{26}\text{Ne}^{5+}$  was selected because there is no lower-mass contaminant with the same  $M/Q = 26/5$  ratio. A solid cryogenic  $^2\text{H}$  target (1 mm thick, 17 mg/cm<sup>2</sup>) developed at GANIL [14,15] was used. The choice of the target thickness results from a compromise between the low intensity and the low energy of the incoming  $^{26}\text{Ne}$  beam.

Beamlike ejectiles were detected and identified with the VAMOS magnetic spectrometer [16,17]. VAMOS has a large momentum acceptance ( $\pm 5\%$ ) and a large angular acceptance with a maximum of  $8^\circ$  (140 mrad) in the laboratory frame in the horizontal and vertical planes. In our experiment, the angular domain is restricted to  $[0^\circ, 3^\circ]$  for the  $(d, p)$  channel, due to the strongly inverse kinematics. Due to a geometrical cut by the beam pipe from the reaction chamber to the entrance of VAMOS, the polar angular acceptance was additionally limited to  $2.7^\circ$ . The resulting cut was checked to be sharp. The detection of VAMOS was composed of two drift chambers to measure the kinematic properties of the ejectiles after the dipole, an ionization chamber for energy-loss measurements ( $\Delta E$ ) and a scintillating plastic detector used to trigger the electronics. A time of flight (TOF) was measured between the plastic scintillator and a microchannel plate device (MCP) located upstream of the target (see Fig. 1). This detection has been designed for low-energy ejectiles by minimizing the windows along the ion path: the two drift chambers [18]

\*Present address: Departamento de FAMN, Universidad de Sevilla, E-41080 Sevilla, Spain.

†Present address: Centre d'Etudes Nucléaires de Bordeaux-Gradignan, F-33175 Gradignan Cedex, France.

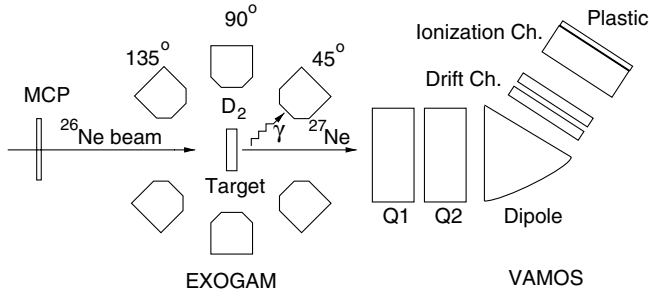


FIG. 1. Experimental setup in the VAMOS vault.

are juxtaposed so that they are constituted by one volume of isobutane delimited by only two  $0.9\text{-}\mu\text{m}$ -thick Mylar windows. The ionization chamber has only one entrance Mylar window ( $1.5\ \mu\text{m}$  thick), the plastic detector being glued to the exit of the chamber. The magnetic rigidity of VAMOS was centered on  $B\rho_0 = 1.0\ \text{Tm}$ . Ejectiles were identified in the focal plane with the horizontal position  $X_f$ , the TOF, and the energy loss  $\Delta E$ . A  $Z$  identification plot from  $\Delta E$ -TOF correlations is shown in Fig. 2: neon and sodium isotopes are produced and clearly separated. A direct  $A/Q$  assignment was done via TOF- $X_f$  correlations [12].

Both singles and events in coincidence with deexcitation  $\gamma$  rays were measured.  $\gamma$  rays were measured with the EXOGAM  $\gamma$  spectrometer [19] surrounding the target (see Fig. 1). In this experiment, 11 clovers (8 EXOGAM clovers and 3 EUROGAM size detectors) were positioned in the array at distances ranging from 11 to 17 cm from the center of the target. Four of them were located at forward angles in a  $45^\circ$  ring, 4 at  $90^\circ$  and 3 at backward angles in a  $135^\circ$  ring. Each clover consists of  $4 \times 4$ -fold segmented germanium crystals. The intrinsic energy resolution of the whole system was  $2.6\ \text{keV}$  full width at half maximum (FWHM) for a  $1332\text{-keV}$   $\gamma$  transition, and its photopeak efficiency for the same transition was determined to be  $4.8\%$ . A time measurement between the central-contact discriminators of EXOGAM and the plastic scintillator of VAMOS is used to select the true

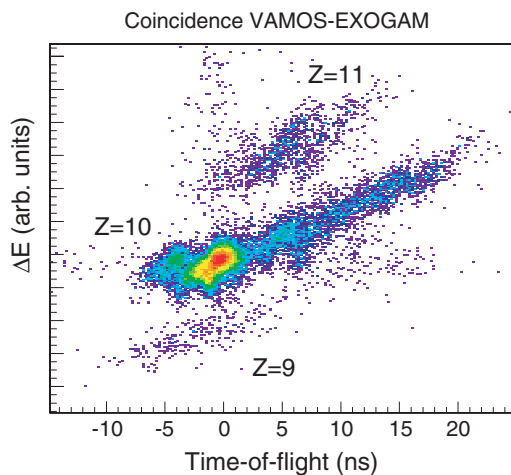


FIG. 2. (Color online)  $\Delta E$ -TOF identification plot for  $Z$  assignment. Only events in coincidence with a  $\gamma$  ray detected in EXOGAM are presented. A part of the total statistics is shown.

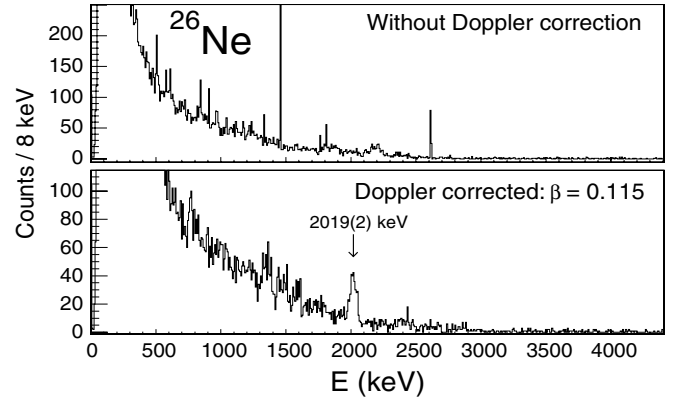


FIG. 3.  $\gamma$ -ray spectrum of  $^{26}\text{Ne}$  without (top) and with (bottom) Doppler correction. Sharp lines in the uncorrected Doppler spectrum are due to well-known transitions from room background.

coincidences and subtract the background due to random coincidences.

### III. RESULTS AND DISCUSSION

#### A. Test case: $^{26}\text{Ne}$

The first  $2^+$  excited state of  $^{26}\text{Ne}$  is well established at  $2018\ \text{keV}$  and has been used to validate the whole setup and analysis method. Excited states of  $^{26}\text{Ne}$  were populated via  $(d, d')$  and inelastic excitation in the Mylar windows of the target. The  $\gamma$ -ray spectrum of  $^{26}\text{Ne}$  is shown in Fig. 3, without (top) and with (bottom) Doppler correction. In the uncorrected spectrum, the intense low-energy exponential background and sharp lines are due to random coincidences, the noninteracting  $^{26}\text{Ne}$  beam being transmitted to the focal plane. It is not observed in the case of transfer-reaction products.

The energy  $E_\gamma$  was measured from the central-contact electrode of the hit crystal. The emission angle  $\theta$  was determined as the polar angle from the beam axis of the segment collecting the highest energy in the considered crystal. Addback corrections for Compton events were also performed when two adjacent crystals of a detector were hit in the same event. As the reaction vertex in the target is not reconstructed, only the mean value of the velocity  $\beta$  was used. For example, the  $^{26}\text{Ne}$  beam is slowed down in the  $^2\text{H}$  target from  $\beta = 0.142$  to  $\beta = 0.090$ . For  $^{26}\text{Ne}$ , a mean velocity  $\beta = 0.115$  was adopted, because for that value the Doppler corrected energies are the same at forward and backward angles for the well-known transition  $2^+ \rightarrow 0^+$  at  $2.02\ \text{MeV}$ , as illustrated in Fig. 4. Assuming a locally linear background, a Gaussian fit gives an energy of  $2019(2)\ \text{keV}$  and a width of  $49(4)\ \text{keV}$  FWHM. The observed transition corresponds to the  $\gamma$  decay of the first  $2^+$  state. Our measurement is in agreement with the  $2018.2(1)\ \text{keV}$  [20] and  $2024(5)\ \text{keV}$  [21] excitation energies previously measured. Estimated contributions to the width are gathered in Table I for both backward and forward angles. The main contribution comes from the large change of the velocity in the target due to the target thickness and the low-energy beam. The final estimated width (taken as the mean value between the  $45^\circ$  and  $135^\circ$  estimations) is  $42\ \text{keV}$  FWHM, in agreement with the

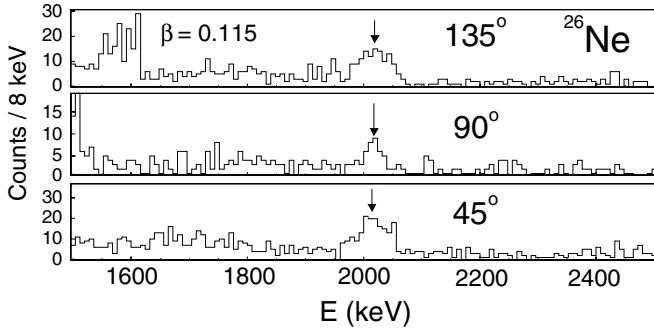


FIG. 4. Doppler corrected deexcitation  $\gamma$ -ray spectrum of  $^{26}\text{Ne}$  for the three detection angles :  $45^\circ$  (bottom),  $90^\circ$  (middle), and  $135^\circ$  (top). The structure at  $\sim 1600$  keV in the  $135^\circ$  spectrum comes from the Doppler correction of the 1460-keV background transition.

49(4) keV measured width. The  $^2\text{H}(^{26}\text{Ne}, ^{26}\text{Ne})^2\text{H}'$  inelastic scattering allowed us to validate the Doppler reconstruction.

### B. $^2\text{H}(^{26}\text{Ne}, ^{27}\text{Ne})^1\text{H}$

We performed the spectroscopy of  $^{27}\text{Ne}$  below its neutron separation threshold  $S_n = 1.43(11)$  MeV [12]. From the measurement of low-energy  $\gamma$  transitions in  $^{27}\text{Ne}$ , constraints on the multipolarity of these transitions and cross sections quantifying the selectivity of the ( $d, p$ ) transfer reaction, we proposed a negative parity to a low-lying level at 765 keV with a spin  $J^\pi = (1/2, 3/2, 5/2)^-$ . Considering all existing data [12,22,23], the most likely assignment is  $J^\pi = 3/2^-$  from the neutron  $p_{3/2}$  orbital. This observation shows that the gap between the  $sd$  and  $fp$  shell is considerably reduced in  $^{27}\text{Ne}$  compared to stable  $N = 17$  isotones. More experimental information on  $^{27}\text{Ne}$  would help to understand the underlying shell structure: (i) the location of its first  $7/2^-$  excited state, distant of less than 1 MeV from the first  $3/2^-$  in all other  $N = 17$  isotones, and (ii) the quadrupole moment of its mass and charge distributions.

### C. $^2\text{H}(^{26}\text{Ne}, ^{25}\text{Ne})^3\text{H}$

A detailed spectroscopy of  $^{25}\text{Ne}$  is useful to test the validity of the  $sd$  shell-model space for its low-lying excitations. Shell-model calculations with the USD interaction [24] predict

TABLE I. Contributions to the width of the 2019-keV peak of Fig. 3: the intrinsic energy resolution  $\delta E_\gamma$ , the velocity uncertainty  $\delta\beta$ , the angular uncertainties  $\delta\theta$  due to the finite size of the segments and the scattering angle of  $^{26}\text{Ne}$ .

Angle	$45^\circ$	$135^\circ$
$\delta E_\gamma$ (keV)	3.6	4.2
$\delta\beta$ (keV)	34.4	40.6
$\delta\theta(\text{segments})$ (keV)	18.6	15.8
$\delta\theta(^{26}\text{Ne})$ (keV)	6.2	5.3
FWHM (keV)	39.8	44.1

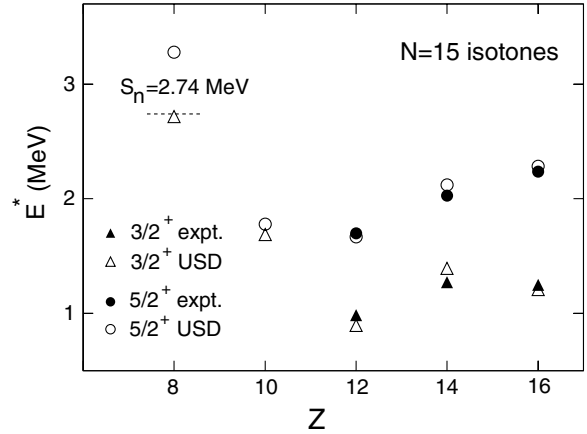


FIG. 5. Comparison between published excitation energies [31] of the first  $3/2^+$  and  $5/2^+$  excited states above a  $1/2^+$  ground state for  $N = 15$  odd isotones and USD predictions.

a ( $3/2^+, 5/2^+$ ) doublet in  $^{25}\text{Ne}$  at 1687 and 1778 keV, respectively. In this section, we provide new elements to determine the levels that correspond to this doublet. The  $3/2^+$  state is described as a  $vd_{3/2}$  neutron configuration, whereas the  $5/2^+$  state results mainly from the coupling of the neutron shell-model state  $vs_{1/2}$  to a  $2^+$  proton excitation of the core. The structure of this  $5/2^+$  state and of the  $3/2^+$  first excited state are very different from each other. The ( $d, t$ ) reaction from  $^{26}\text{Ne}$  is then expected to be very selective and strongly favors hole states in  $^{25}\text{Ne}$  like the  $5/2^+$  state of the doublet. The spectroscopic factor from  $^{26}\text{Ne}(\text{gs})$  to the  $5/2^+$  state of  $^{25}\text{Ne}$  is predicted to be 2.3 from USD shell-model calculations, whereas the spectroscopic factor to the first  $3/2^+$  state is 0.4 [29].

Figure 5 shows the systematics of the first  $3/2^+$  and  $5/2^+$  excited states in  $N = 15$  odd isotones. USD calculations are compared to available data: for isotones with  $Z > 10$ , the agreement is very good and suggests a good prediction for  $^{25}\text{Ne}$ . Spectroscopic information about  $^{25}\text{Ne}$  have been reported from the  $\beta$  decay of  $^{25}\text{F}$  [20,25], from low-energy transfer reactions  $^{26}\text{Mg}(^7\text{Li}, ^8\text{B})^{25}\text{Ne}$  [26],  $^{26}\text{Mg}(^{13}\text{C}, ^{14}\text{O})^{25}\text{Ne}$  [27], and the one-neutron pickup  $^2\text{H}(^{24}\text{Ne}, ^{25}\text{Ne})^1\text{H}$  [28], and also from higher incident-energy reactions: the one-neutron removal  $^9\text{Be}(^{26}\text{Ne}, ^{25}\text{Ne})\text{X}$  [23,29] and the breakup of  $^{26}\text{Ne}$  on  $^{208}\text{Pb}$  [30]. A comparison of most of the previous data and shell-model calculations within the  $sd$  shell-model space are shown in Ref. [25]. In the aforementioned experiments, no doublet was observed in the 1700-keV region within a range of 300 keV. The multinucleon transfers [26] and [27] were limited by an energy resolution not better than 100 keV. The suggestion of a doublet in Ref. [27] was not confirmed in more recent  $\beta$  decay of  $^{25}\text{F}$  [20,25] with a much better resolution (a few keV). In Ref. [25], a 2096-keV transition has been confirmed, and the authors concluded that the USD doublet states correspond to excited states at 1702 and 2096 keV. These conclusions rely on  $\log(ft)$  measurements and multipolarity constraints.

The  $\gamma$ -ray spectrum of  $^{25}\text{Ne}$  obtained in this experiment is shown in Fig. 6: without (top) and with (bottom) Doppler cor-

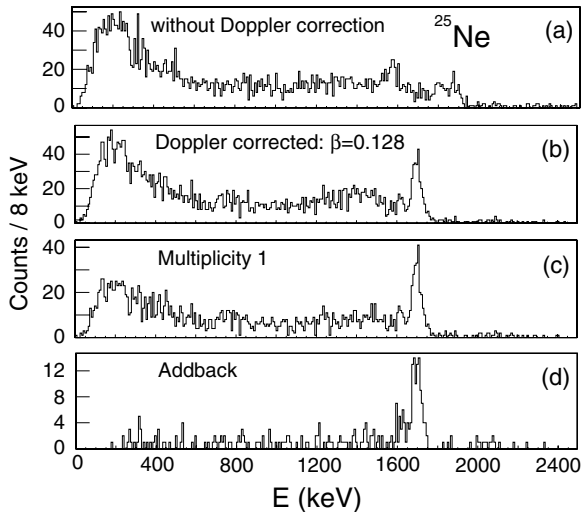


FIG. 6.  $\gamma$ -ray spectra of  $^{25}\text{Ne}$ : without Doppler correction (a), Doppler corrected with a velocity  $\beta = 0.128$  (b), multiplicity 1 events only (c), and addback events (d).

reaction with a velocity of  $\beta = 0.128$ . The corrected spectrum is divided into three distinct energy regions: around 1700 keV where a group of transitions is visible, a region with a very few counts at high energy and the low-energy part dominated by Compton events from higher-energy transitions. In Fig. 7, these

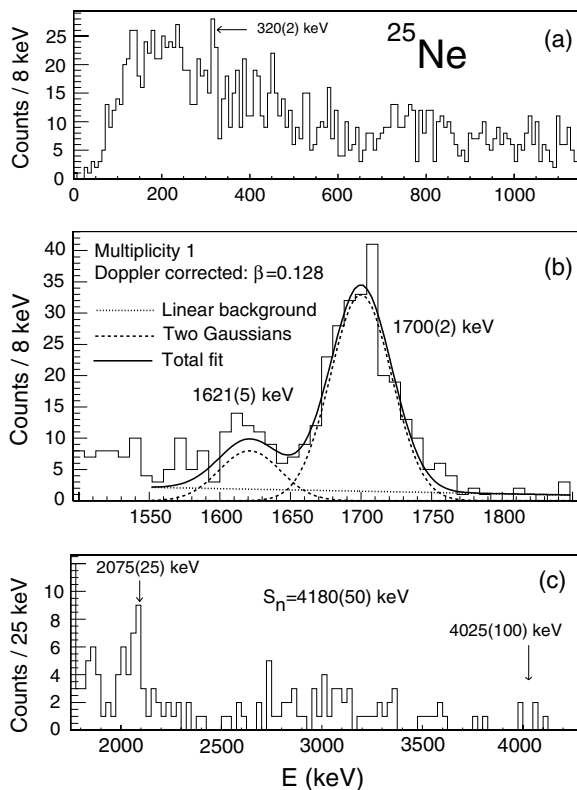


FIG. 7.  $\gamma$  spectrum of  $^{25}\text{Ne}$ . (a) The low-energy part of the spectrum shows a 320-keV transition, present in all angular rings. (b) Zoom of the 1700-keV region: the result of the fit for two transitions at 1621 and 1700 keV is shown. (c) High-energy region: the low background allows for sensitivity to transitions with low statistics.

TABLE II. Observed transitions in  $^{25}\text{Ne}$  from  $^2\text{H}(^{26}\text{Ne}, ^{25}\text{Ne})^3\text{H}$  (see Fig. 7). The experimental width of each transition is compared to a theoretical evaluation. The theoretical value does not take into account shifts from half-life effects.

$E_\gamma$ (keV)	$\text{FWHM}_{\text{exp}}$ (keV)	$\text{FWHM}_{\text{theo}}$ (keV)
320(2)	5(4)	7
1621(5)	42(4)	36
1700(2)	51(7)	36
2075(25)	38(14)	45
4025(100)	—	87

three regions are shown separately. It is worth noting that only a part of the momentum distribution of  $^{25}\text{Ne}$  was transmitted to the spectrometer. Therefore, we did not measure any absolute cross section for the  $(d, t)$  reaction channel.

A zoom of the 1700-keV region [Fig. 7(b)] shows two structures at  $\sim 1620$  and  $\sim 1700$  keV. We considered two possibilities: one (case 1) or two (case 2) transitions to reproduce the 1700-keV peak. We assumed Gaussian shapes for the transitions over a locally linear background. In case 1 [fit in Fig. 7(b)], the width of the peak is 51 keV FWHM compared to the expected 36-keV value (Table II), whereas a smaller value of 42 keV FWHM is obtained in case 2. However, it is difficult to conclude because a half-life of about 30 ps (the time necessary for  $^{25}\text{Ne}$  to go through the target) is enough to induce a broadening of the peak. Indeed, such a scenario is plausible for the first excited state of  $^{25}\text{Ne}$ : assuming a  $(3/2, 5/2)^+$  state at 1700 keV, the transition to the  $1/2^+$  ground state corresponds to a  $E2$  or  $M1$  transition (or a mixing  $M1/E2$ ) with, according to Weisskopf estimates, a half-life expected to be of the order of 10 ps. That ambiguity combined with rather low statistics prevents any conclusion: no evidence could be found for a doublet at 1700 keV.

The observed 1621(5)-keV transition, consistent with previous measured energies, corresponds to the decay of a 3321(6)-keV state to the 1700(2)-keV level. This 3321-keV excitation energy is in good agreement with the 3324-keV value recently published in Ref. [25] and with similar excitation energies measured via particle transfer in previous experiments [26–28].

The high-energy region of the Doppler-corrected spectrum is shown in the bottom panel of Fig. 7. The statistics are poor, and it is important to determine the random background component at these energies. In the  $\gamma$  spectrum of  $^{27}\text{Ne}$ , 20 counts have been measured above 1800 keV and are considered as background for total statistics of 3654 counts, because the neutron separation energy of  $^{27}\text{Ne}$  is  $S_n = 1.4$  MeV. For  $^{25}\text{Ne}$ , the high-energy spectrum ( $E > 1800$  keV) contains 137 counts for a total amount of 2662 counts. It leads to an estimation of 11% background relative to the total number of counts in the high-energy part of the  $^{25}\text{Ne}$  spectrum by analogy with  $^{27}\text{Ne}$ . It indicates that most of the high-energy counts observed in the spectrum come from the decay of  $^{25}\text{Ne}$ . One transition at 2075(25) keV is clearly visible in the high-energy spectrum of Fig. 7. Its width is consistent with the

theoretical value as indicated in Table II. This transition has already been observed through  $\gamma$  spectroscopy at 2030 [28], 2050(100) [30], and 2090(3) keV [25] and corresponds to the direct decay of a level observed via ( $^7\text{Li}, ^8\text{B}$ ) and measured by missing-mass measurement at 2030 keV [26]. This state has been proposed to correspond to the  $3/2^+$  state of the USD doublet [25]. From the selectivity of the ( $d, t$ ) reaction, the ratio of the counts measured at 2075 keV to the counts in the 1700-keV transition is, after correction of the energy efficiencies of EXOGAM, 0.14, very close to the ratio of spectroscopic factors from USD calculations  $S(3/2^+)/S(5/2^+) = 0.16$ . This comparison is a strong argument in favor of the conclusions of [25]: the  $5/2^+$  level of the USD doublet lies at 1700 keV, whereas the  $3/2^+$  lies at 2075(25) keV. The events whose energy is above 2500 keV are not directly assignable to transitions because the statistics are low. Nevertheless, we observe an amount of counts centered at 3000 keV that indicates the presence of high-energy states produced during the reaction. Five events are measured around 4025(100) keV, suggesting a possible direct branch to the ground state for the level(s) previously assigned at  $\sim 4050$  keV [20,26–28].

The low-energy part of the  $\gamma$  spectrum of  $^{25}\text{Ne}$  is mainly composed of Compton events from high-energy transitions. Among the low-energy part of Fig. 7, we identified one transition present over a large background in every angular detection ring at 320(2) keV. This transition is reported in Table II with all the other measured transitions. This transition cannot be assigned to a specific level decay in this work and has not been observed in  $\beta$ -decay experiments despite a good energy resolution and low background. From this comparison, we can infer that the level scheme of  $^{25}\text{Ne}$  may contain more levels than observed in  $\beta$ -decay experiments as suggested by shell-model calculations. Conversely, we do not observe the 574- and 2186-keV transitions that are suggested by a  $\beta$ -decay experiment [25] to correspond to the decay of a 3889-keV level. This indicates that this state, not produced via ( $d, t$ ), is not a neutron-hole excitation. The other structures in the low-energy spectrum of  $^{25}\text{Ne}$  are not present in all the angular rings and, therefore, are not considered as transitions. The level scheme obtained from this experiment is presented in Fig. 8 and compared to shell-model calculations performed with the USD interaction.

Finally, we observed three already-known transitions in  $^{25}\text{Ne}$  produced from  $^2\text{H}(^{26}\text{Ne}, ^{25}\text{Ne})^3\text{H}$ : 1700(2), 2075(25), and 1621(5) keV, which correspond to the decay of excited states at 1700, 2075, and 3321 keV, respectively. The 2075-keV transition is consistent with the 2090-keV transition observed in  $\beta$  decay [25]. The selectivity of the ( $d, t$ ) reaction, in comparison with spectroscopic factors from USD calculations, gives a strong argument to assess  $J^\pi = 5/2^+$  to the 1700-keV level, and  $J^\pi = 3/2^+$  to the 2075-keV state, as previously proposed [25]. High-energy counts at 4025(100) keV may indicate a branch for the direct  $\gamma$  decay of the already known 4050 keV excited state to the ground state. The obtained level scheme from one-neutron stripping is consistent with shell-model calculations performed within the  $sd$  shell-model space, showing no evidence for a strong component with low-lying  $fp$  orbitals in the  $^{26}\text{Ne}$  ground-state wave function. These  $fp$  orbitals do not seem to strongly influence the low-lying spectroscopy of  $^{25}\text{Ne}$ .

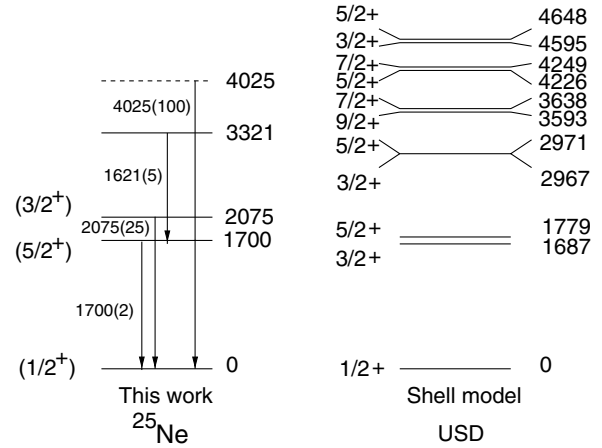


FIG. 8. Levels of  $^{25}\text{Ne}$  observed in  $^2\text{H}(^{26}\text{Ne}, ^{25}\text{Ne})^3\text{H}$ . Prediction from shell-model calculations performed with the USD interaction are also presented.

Going toward the neutron drip line along the neon isotopic chain, they appear to result in a negative-parity excited state at 765 keV in  $^{27}\text{Ne}$  [12] with a substantial amount in the ground state of  $^{28}\text{Ne}$  [23], and they are suggested to be intruders in the ground state of  $^{30}\text{Ne}$  [6].

#### D. Sodium isotopes

In addition to neon isotopes, we have studied the spectroscopy of sodium isotopes with  $N = 15$  and  $N = 16$ . Their spectroscopy, by comparison to USD shell-model calculations, tests also the validity of the  $sd$  shell-model space in that region of the nuclear chart.

##### I. $^{27}\text{Na}$

The lowest excited states in  $^{27}\text{Na}$  still present some uncertainty on their spin and parity assignment. The spectroscopy of  $^{27}\text{Na}$  has already been studied via multinucleon transfer from  $^{26}\text{Mg}$  [32,34] and  $^{14}\text{C}$  [33].  $^{27}\text{Na}$  ground state is known to be  $5/2^+$  from laser spectroscopy [35] and  $\beta$  decay [36]. A low-lying  $3/2^+$  at 62 keV above the ground state has also been identified in Ref. [33]. Two transitions at 1663 and 1753 keV have been assigned to low-lying states at 1725 and 1815 keV that both decay to the 62-keV state, respectively. These states have been proposed to be  $1/2$  levels [33] from angular-momentum selection rules and  $\gamma$  angular distribution for the 1663-keV transition. The parity assignment of these two states was made supposing that one of the states is the  $1/2^+$  state predicted by USD shell-model calculations and that the other state is a  $1/2^-$  intruder state from the proton  $p$  shell. The reaction  $^{26}\text{Mg}(^{18}\text{O}, ^{17}\text{F})^{27}\text{Na}$  [32] populates significantly the 1725-keV level. M. W. Cooper *et al.* suggested that the 1725-keV level is a  $1/2^-$  state without excluding the opposite parity assignment [33]. In the following we resolve this uncertainty on the parity of the first  $1/2$  state.

The  $\gamma$  spectrum of  $^{27}\text{Na}$  is shown in Fig. 9, where the Doppler correction is performed with a velocity of  $\beta = 0.105$ .

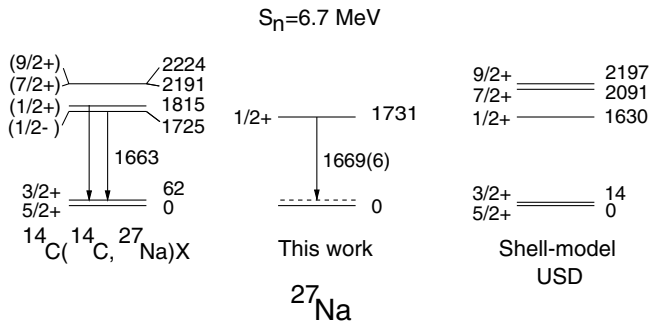
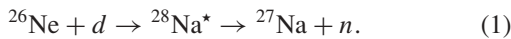


FIG. 9. Comparison of the present results among the  $^{27}\text{Na}$  level scheme, published data, and USD calculations.

One transition is visible at 1669(6) keV, in agreement with the 1663-keV transition observed in Ref. [33]. Its width is 30(7) keV, consistent with the theoretical estimation of 30 keV. The observed transition is then identified as the decay of the 1725-keV level to the low-lying  $3/2^+$  excited state at 62 keV. The energy threshold of the EXOGAM array was too high to detect this low-energy transition. The statistics at higher energy is too low to identify any other excited state.

It is important to determine the mechanism responsible for the production of  $^{27}\text{Na}$  to interpret properly the population of the mentioned excited state. We now show that the observed  $^{27}\text{Na}$  are mainly produced by a direct ( $d, n$ ) transfer reaction. The production of  $^{27}\text{Na}$  from  $^{26}\text{Ne}+d$  may have two different origins: the direct ( $d, n$ ) reaction or a fusion-evaporation process



Nevertheless, two arguments are in favor of a direct reaction. (i) The very clean  $\gamma$  spectrum suggests that the mechanism to produce  $^{27}\text{Na}$  from  $^{26}\text{Ne}+d$  was selective and may be considered as a direct ( $d, n$ ) reaction. Indeed, a fusion-evaporation process implies a statistical feeding of the excited states. As a statistical feeding depends mainly on the excitation energy and the spin of the concerned states, the two states at 1815 and 1725 keV should be fed at the same level from the statistical part of the feeding because they are almost at the same excitation energy and both assigned to have a spin 1/2. The lack of the 1753-keV transition, corresponding to the decay of the 1815-keV state to the 62-keV low-lying level, compared to the population of the 1669-keV level indicates that the population of the 1/2 states is not driven by a statistical law. (ii) The fusion  $Q_f$  value is positive:  $Q_f = 14.2$  MeV.

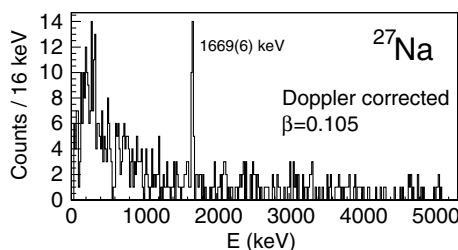


FIG. 10. Doppler-corrected  $\gamma$  spectrum of  $^{27}\text{Na}$ . The neutron separation energy of  $^{27}\text{Na}$  is  $S_n = 6.726(7)$  MeV [37].

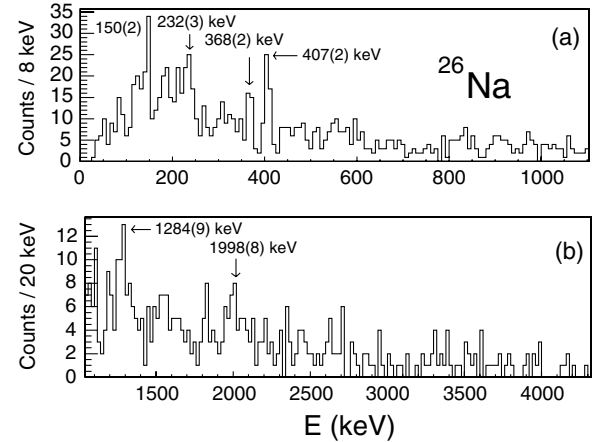


FIG. 11. Low-energy (a) and high-energy (b) part of the  $\gamma$  spectrum of  $^{26}\text{Na}$ . The spectrum is Doppler corrected with a velocity  $\beta = 0.095$ . The neutron separation energy of  $^{26}\text{Na}$  is  $S_n = 5.576(6)$  MeV [37].

In the case of the experiment, the kinematics imply an excitation energy of 33 MeV for  $^{28}\text{Na}$ . This excitation energy is very high compared to the one- and two-neutron separation energy of  $^{28}\text{Na}$  [ $S_n = 3.52(8)$  MeV,  $S_{2n} = 10.37(8)$  MeV], showing that the one-neutron evaporation is not expected to be a favored decay of the compound  $^{28}\text{Na}$ . We then assume that  $^{27}\text{Na}$  was mainly produced via the direct ( $d, n$ ) reaction.

The populated levels produced from ( $d, n$ ) should be proton particle states. This picture for the observed excited state is confirmed by a shell-model calculation within the  $sd$  shell-model space with the USD interaction in which a  $1/2^+$  state is predicted at 1630 keV and described as a single-particle state with a  $\pi(d_{5/2})^2(s_{1/2})^1$  main configuration. Our data indicate then that the 1725-keV state is a  $1/2^+$  level (see Fig. 10).

## 2. $^{26}\text{Na}$

$^{26}\text{Na}$  has already been studied from transfer reactions [38–40] and  $\beta$  decay of  $^{26}\text{Ne}$  [41]. Recently, a detailed spectroscopy has been obtained from  $^{14}\text{C}(^{14}\text{C}, d)^{26}\text{Na}$  [42]. In our case, the origin of  $^{26}\text{Na}$  observed in the focal plane may be due to a charge exchange process or fusion followed by the evaporation of two neutrons, with a cross section expected to be two orders of magnitude higher in the latter case [43,44]. No spectroscopic selectivity in the population of the different states is therefore expected.

The following transitions (quoted by arrows in the Doppler-corrected spectrum of Fig. 11) have been checked to be present in all the  $\gamma$ -detection angular rings to eliminate spurious peaks: 150(2), 232(3), 368(2), 407(2), 1284(9), and 1998(8) keV. Except for the 368-keV transition, these results are a confirmation of the transitions observed in Ref. [42] by another reaction channel.

## IV. CONCLUSION

We performed the  $\gamma$  spectroscopy of the neutron-rich nuclei  $^{25,27}\text{Ne}$  and  $^{26,27}\text{Na}$  from the reaction of  $^{26}\text{Ne}$  with deuterium in inverse kinematics at 9.7 MeV/nucleon. The use

of a cryogenic  $\text{D}_2$  target with the  $\gamma$  spectrometer EXOGAM coupled to the magnetic spectrometer VAMOS gives access to deuteron-induced reaction and allows the high-resolution  $\gamma$  spectroscopy of the reaction products even with a low-intensity beam (3000 pps of  $^{26}\text{Ne}$  in this experiment). For  $^{25}\text{Ne}$  produced via the one-neutron removal  $^2\text{H}(^{26}\text{Ne}, ^{25}\text{Ne})^3\text{H}$ , no evidence for a doublet at 1700 keV is found, consistently with the conclusions of  $\beta$ -decay experiments [20,25]. A 2075(25)-keV level is confirmed and suggested to have  $J^\pi = 3/2^+$ . A spin and parity  $J^\pi = 5/2^+$  is assigned to the 1700-keV state. The observation of an unassigned transition at 320(2) keV and a consequent amount of high-energy  $\gamma$  rays may sign the existence of bound high-energy excited states in  $^{25}\text{Ne}$  produced by neutron stripping. The relatively good agreement between shell-model calculations for  $^{25}\text{Ne}$  and the known levels of  $^{25}\text{Ne}$  may indicate that the  $sd$ - $fp$  shell gap is rather large in  $^{25}\text{Ne}$ . In the present experiment, low-lying

intruder states below 1 MeV have been observed in  $^{27}\text{Ne}$  [12]. In addition to recent conclusions for  $^{28}\text{Ne}$  [22,23], these results show that the intrusion of  $fp$  orbitals in the low-lying spectroscopy of neon isotopes occurs around  $N = 17$ . For  $^{27}\text{Na}$ , the selectivity of the  $(d, n)$  transfer reaction allowed us to assign a  $1/2^+$  spin and parity to the 1731(6)-keV state, showing a good agreement with  $sd$  shell-model calculations.

#### ACKNOWLEDGMENTS

We acknowledge the technical staffs of GANIL for their excellent support: P. Dolégiéviez, P. Gallardo, and P. Robillard for the cryogenic target; J. Ropert and G. Voltolini for EXOGAM; and B. Lecornu and C. Mary for VAMOS. We also acknowledge the beam delivery teams of SPIRAL for the high quality of their work.

- 
- [1] C. Thibault *et al.*, Phys. Rev. C **12**, 644 (1975).  
[2] N. Orr *et al.*, Phys. Lett. **B258**, 29 (1991).  
[3] C. Détraz *et al.*, Phys. Rev. C **19**, 164 (1979).  
[4] T. Motobayashi *et al.*, Phys. Lett. **B346**, 9 (1995).  
[5] A. Watt *et al.*, J. Phys. G **7**, L145 (1981).  
[6] Y. Yanagisawa *et al.*, Phys. Lett. **B566**, 84 (2003).  
[7] A. Ozawa *et al.*, Phys. Rev. Lett. **84**, 5493 (2000).  
[8] M. Stanoiu *et al.*, Phys. Rev. C **69**, 034312 (2004).  
[9] M. Beiner, R. J. Lombard, and D. Mas, Nucl. Phys. **A289**, 1 (1975).  
[10] T. Otsuka *et al.*, Phys. Rev. Lett. **87**, 082502 (2001).  
[11] A. Obertelli *et al.*, Phys. Rev. C **71**, 024304 (2005).  
[12] A. Obertelli *et al.*, Phys. Lett. **B633**, 33 (2006).  
[13] A. C. Villari *et al.*, Nucl. Phys. **A693**, 465 (2001).  
[14] P. Dolégiéviez *et al.*, Cryogenic system for a thin solid hydrogen target, Report Ganil A 00 01, November 29, 2000.  
[15] P. Dolégiéviez *et al.*, Nucl. Instrum. Methods A **564**, 32 (2006).  
[16] H. Savajols (VAMOS Collaboration), Nucl. Phys. **A654**, 1027c (1999).  
[17] R. Anne, *Proceedings of EXON 2001*, edited by E. Penionzhkevich and E. A. Cherepanov (World Scientific, Singapore, 2001).  
[18] E. Bougamont, internal report CEA/DSM/DAPNIA, ref. 6D6810E2100/303 (2002).  
[19] <http://www.ganil.fr/exogam>.  
[20] A. T. Reed *et al.*, Phys. Rev. C **60**, 024311 (1999).  
[21] M. Belleguic *et al.*, Phys. Rev. C **72**, 054316 (2005).  
[22] Zs. Dombradi *et al.*, Phys. Rev. Lett. **96**, 182501 (2006).  
[23] J. R. Terry *et al.*, Phys. Lett. **B640**, 86 (2005).  
[24] B. A. Brown and B. H. Wildenthal, Annu. Rev. Nucl. Part. Sci. **38**, 29 (1988).  
[25] S. W. Padgett *et al.*, Phys. Rev. C **72**, 064330 (2005).  
[26] K. H. Wilcox *et al.*, Phys. Rev. Lett. **30**, 866 (1973).  
[27] C. L. Woods *et al.*, Nucl. Phys. **A476**, 392 (1988).  
[28] W. N. Catford *et al.*, J. Phys. G **31**, S1655 (2005).  
[29] J. R. Terry and J.-L. Lecouey, Nucl. Phys. **A734**, 469 (2004).  
[30] J. Gibelin *et al.*, RIKEN Accel. Prog. Rep. **37**, 53 (2004).  
[31] P. M. Endt, Nucl. Phys. **A521**, 1 (1990).  
[32] L. K. Fifield *et al.*, Nucl. Phys. **A437**, 141 (1985).  
[33] M. W. Cooper *et al.*, Phys. Rev. C **65**, 051302(R) (2002).  
[34] I. Paschopoulos *et al.*, Phys. Rev. C **18**, 1277 (1978).  
[35] G. Huber *et al.*, Phys. Rev. C **18**, 2342 (1995).  
[36] D. E. Alburger, D. R. Goosman, and C. N. Davids, Phys. Rev. C **8**, 1011 (1973).  
[37] LBNL Isotopes Project Nuclear Data Dissemination Home Page. Retrieved March 11, 2002, from <http://ie.lbl.gov/toi.html>.  
[38] E. R. Flynn and J. D. Garrett, Phys. Rev. C **9**, 210 (1974).  
[39] K. I. Pearce *et al.*, Phys. Rev. C **35**, 1617 (1987).  
[40] H. Scheit *et al.*, nucl-ex/0401023, 01/21/2004 (2004).  
[41] L. Weissman *et al.*, Phys. Rev. C **70**, 057306 (2004).  
[42] Sangjin Lee *et al.*, Phys. Rev. C **73**, 044321 (2006).  
[43] E. R. Flynn, J. Sherman, and N. Stein, Phys. Rev. Lett. **32**, 846 (1974).  
[44] D. Ridikas *et al.*, Phys. Rev. C **63**, 014610 (2000).